Journal of Power Sources 227 (2013) 237–242

Contents lists available at SciVerse ScienceDirect

Journal of Power Sources

journal homepage: www.elsevier.com/locate/jpowsour

Nanoscale compositional changes during first delithiation of Si negative electrodes

Magali Gauthier [a,b], Julien Danet [c], Bernard Lestriez [a], Lionel Roué [b], Dominique Guyomard [a], Philippe Moreau [a,*]

[a] Institut des Matériaux Jean Rouxel (IMN), Université de Nantes, CNRS, 2 rue de la Houssinière, BP 32229, 44322 Nantes Cedex 03, France
[b] INRS-Énergie, Matériaux et Télécommunications, 1650 boulevard Lionel Boulet, Varennes, Québec, J3X 1S2, Canada
[c] CEA Grenoble, DRT/LITEN/DEHT/LMB, 17 rue des martyrs, 38054 Grenoble cedex 9, France

HIGHLIGHTS

- A biphasic process for $x > 2$ followed by a solid solution is proven for delithiation.
- Both nano- and micro-Si present the same behaviour.
- In electrodes prepared with nano-silicon, nanoscale inhomogeneities can be large.
- These inhomogeneities decrease as delithiation increases.
- Inhomogeneities through the electrode thickness are relatively small.

GRAPHICAL ABSTRACT

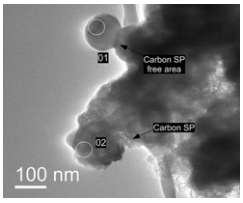

ARTICLE INFO

Article history:
Received 1 August 2012
Received in revised form
9 October 2012
Accepted 16 November 2012
Available online 24 November 2012

Keywords:
Li-ion battery
Silicon electrode
Nano-analysis
Li–Si alloy
Electron energy-loss spectroscopy
Homogeneity

ABSTRACT

The local composition of negative silicon electrodes is studied by *ex situ* electron energy-loss spectroscopy along the first delithiation in a lithium battery. By measuring dozens of sample areas for over a dozen compositions, the local and overall inhomogeneities in these practical electrodes are evaluated. The statistical treatment of the data highlights the existence of larger inhomogeneities at the beginning of the delithiation as well as at a 100 nm scale. It is also shown that, even if incremental capacity curves are different, the compositional changes during delithiation are identical for nano- and micro-Si. Namely, an initial $Li_{15}Si_4$ phase is replaced by a $Li_{2\pm0.3}Si$ amorphous phase in a biphasic process, the latter compound being further delithiated to amorphous silicon in single phase process. Results also show that the electrochemical irreversibility associated with the liquid electrolyte reduction/degradation is generated during the lithiation process, not the delithiation process.

1. Introduction

The considerable interest generated by the use of silicon as a negative electrode for Li-ion batteries has not diminished since the detailed studies conducted at the turn of the century [1–3]. Electrodes developed in this context, however, were not able to produce sufficiently reversible reactions beyond a few cycles due to the large volume change that occurs during the alloying/dealloying process. The design of the composite electrode architecture and the selection of suitable binders contributed to the production of current day electrodes displaying improved, if not entirely satisfactory, performance [4,5].

* Corresponding author. Tel.: +33 (0) 240376414; fax: +33 (0) 240373995.
E-mail address: philippe.moreau@cnrs-imn.fr (P. Moreau).

0378-7753/$ – see front matter © 2012 Elsevier B.V. All rights reserved.
http://dx.doi.org/10.1016/j.jpowsour.2012.11.047

A better knowledge of the processes of amorphisation and crystallisation of phases using techniques such as X-ray diffraction has since been achieved [6]. This information was particularly important due to the particular mechanism involved, i.e. the first lithiation of crystalline silicon is very different from the subsequent ones. After the first lithiation, cycling occurs on an amorphous phase [2], except at the end of discharge (full lithiation), where the formation of a $Li_{15}Si_4$ phase, not present in the Li–Si phase diagram, is observed [7]. The presence of such a crystalline phase is believed to decrease the reversibility of the charge–discharge processes [7,8]. Apart from this $Li_{15}Si_4$ phase, complete cycling involves phases which are amorphous at the X-ray diffraction scale. If one is to make progress with respect to the determination of phases during the major part of cycling, as well as their local distribution and interaction in the composite electrode at the nanoscale, it has long been agreed that Transmission Electron Microscopy (TEM) is a technique to be privileged [1,2]. The latest *in situ* experiments open up even more possibilities [9,10]. Lithium is, however, a difficult atom to detect, especially in an amorphous environment [11]. Electron energy-loss spectroscopy has been shown to be well adapted to analyse lithium-containing compounds [12,13]. In the case of Li_xSi alloys, particularly, it has recently been demonstrated that the plasmon region (around 20 eV in the energy-loss spectrum) is precise enough to determine local compositions [14]. Danet et al. showed that, during the first lithiation, the crystalline silicon is in equilibrium with a $Li_{2.9}Si$ amorphous phase. The database created on plasmon energies of Li_xSi alloys was used to arrive at this conclusion. This study seemed also to indicate a nucleation process, and an overlithiation was observed at the end of the discharge. At a nanoscale, these results complement others inferred from X-ray diffraction [6] and NMR techniques [15].

The first charge is a critical moment in the cycling process as it follows the creation of the initial SEI and therefore has to absorb for the first time the dramatic decrease in volume of the alloy. The purpose of this paper is to analyse the local compositional changes during the first charge and provide information on the initial irreversibility, by the use of the EELS technique already validated on the first lithiation. To this end, particular attention was paid to the statistical treatment of the EELS data. Our findings show that, at a nanoscale, a Li_2Si phase is rapidly formed upon delithiation of a fully lithiated silicon electrode, regardless of which crystalline silicon is used (micrometric or nanometric). Further delithiation is shown to proceed via a single phase process.

This study also suggests that, with respect to the nano-size silicon, the non-homogeneity of the electrode at a scale of a few hundred nanometres limits electrode performance.

2. Experimental

The composite electrodes prepared consist of 80% nanometric Si (98%, 50 nm, Alfa Aesar) or micrometric Si (99.9%, 1–5 μm, Alfa Aesar), 12% carbon black (super P, Timcal) and 8% carboxymethylcellulose (DS = 0.7, M_w = 90,000 Aldrich). They were prepared in an aqueous solution by ball milling at 500 rpm for 1 h using a Fritsch Pulverisette 7 apparatus [4]. Slurries were then tape casted onto a 25 μm copper foil, dried at room temperature for 12 h and then under vacuum at 100 °C for 2 h. The resulting active mass loadings of the electrodes ranged from 0.5 to 1.8 mg cm^{-2}. No calendar pressure was used.

Electrochemical tests were performed in two-electrode Swagelok® cells which were assembled in a glove box comprising the composite electrode as the positive electrode, a Whatman GF/D borosilicate glass-fibre separator soaked with a mixture of 1 M $LiPF_6$ dissolved in ethylene carbonate (EC)–dimethyl carbonate (DMC) 1:1 as the electrolyte and lithium metal as the counter and reference electrode. Galvanostatic cycling for nano-Si electrodes was carried out at 20 °C between 1 and 0.005 V vs. Li^+/Li^0 with a VMP system (Biologic) at a C/25 rate in discharge (complete lithiation in 25 h) and a C/100 rate in charge (delithiation in 100 h), based on a theoretical capacity of 3579 mAh g^{-1} corresponding to the formation of the $Li_{15}Si_4$ phase. For micro-Si composite electrodes, a C/25 rate in charge was applied. After cycling, the cells were stopped and immediately disassembled in the glove box, in which electrodes were washed and dispersed in DMC. A drop of the solution was then deposited onto a lacey carbon copper grid, which was placed in a vacuum transfer sample holder (Gatan 626), thus avoiding contact with air during transfer to the transmission electron microscope. The time lapse between cycling stop and the beginning of analysis in the TEM was around 2 hours.

A Hitachi HF2000 TEM equipped with a modified Gatan 666 spectrometer (optically coupled to a CCD camera) was used to perform EELS measurements at 100 kV. The selected probe size was around 50 nm in order to restrain electron beam degradation. EELS data were acquired using 1.4 mrad convergence and 4.55 or 9.09 mrad collection angles. For these high values compared to the characteristic angle of diffusion (≈0.07 mrad), results are not affected by this collection angle. The dispersion was 0.1 eV/pixel and the energy resolution was 0.8 eV. Spectra were corrected for gain variation and dark counts. Deconvolution by the zero loss peak and single scattering spectra were obtained using the PEELS program [16]. For each nano-Si based electrode, five successive spectra with an acquisition time of 1 ms were recorded on the same sample area. A rapid increase of plasmon energy with exposure time is observed (Fig. 1) which, as will be shown later on, indicates a selective loss of lithium. In order to exclude this fast beam damage from our study, only the first two spectra in the series were retained providing that their deviation was less than 0.1 eV (Fig. 1). Taking into account the reading time of the camera, the total exposition time of the area to the electron beam can be estimated to be less than 1 s. Since the beam degradation is lower with micro-Si electrodes, it was usually possible to retain more than the first two spectra with this type of electrode. Between one and two dozen plasmon energy values were obtained for each sample. Spectra were then fitted over the top 30% of the plasmon peak using the Drude model [14,17].

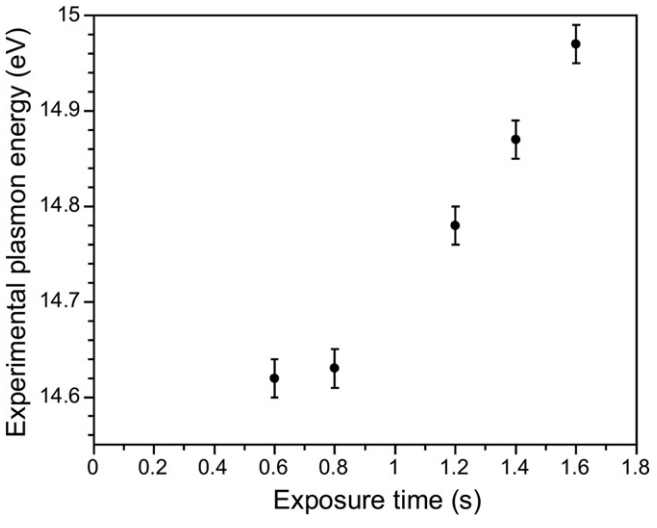

Fig. 1. Evolution during measurement of plasmon energies of a sample showing the fast degradation under the electron beam.

3. Results and discussion

3.1. Compositional homogeneity during delithiation

In this study, 14 compositions along the first charge (delithiation) of Si-based electrodes were investigated using EELS (Table 1). In Fig. 2, the different states of charge studied are marked as dots on typical 1st cycle curves for both nano- and micro-Si. The sizeable dispersion of potential observed for similar apparent compositions might well be explained by the fairly large range of mass loadings. In this same graph, it should be noted that the x values were calculated while taking in account that the discharge of the Si electrodes ends with the formation of the $Li_{15}Si_4$ phase. In this paper, these states of charge will be called the apparent x value since the alloying/dealloying reaction of Li with Si is not fully reversible. There are various causes for the large irreversible capacity in Si electrodes, such as SEI formation [18] or loss of active material [19]. Since the proportions of each phenomenon are unknown, the apparent x value along the charge is only indicative of an approximate composition of the electrode.

In Fig. 3, plasmon energy measurements on the $x = 2.5$ electrode are presented as an example. Around two dozen different areas were investigated on this sample. A rather large dispersion in values is observed, starting from low values corresponding to highly lithiated alloys, up to high values related to pure silicon. This dispersion reflects the fact that, at the nanoscale, the electrochemical process occurring in Si electrodes is not homogeneous. Lithium alloying with Si begins with those particles having better accessibility for both electrons and ions [20]. It can thus be assumed that particles are delithiated differently depending on the quality of their ionic and electronic wiring [21], with a probable faster alloying/dealloying rate near the current collector. Such a situation has often been observed in other electrode materials [22].

In order to check if this observed inhomogeneity is related to the proximity of the analysed particles to the current collector, a special sample preparation was carried out. In the glove box, an electrode corresponding to $x = 2.2$ (nano-Si) was first polished to remove its surface. The small quantity of electrode left on the current collector was then recovered, deposited on a TEM grid and studied by EELS. The $x = 2.2$ polished electrode exhibits an almost identical experimental plasmon energy to that of the $x = 2.3$ electrode prepared with the standard method (Table 1). Inhomogeneities revealed in all these experiments are thus not situated at a macroscale

Table 1
Apparent states of charge (x from electrochemical curves) and corresponding potentials for nano- and micro-Si electrodes; experimental plasmon energies, $\overline{E_p}$, determined using Drude's model and their respective mean standard deviations in brackets; local compositions obtained from EELS and Eq. (1). The values in italic correspond to the electrode scrapped before analysis.

Silicon size	x (electrochem.)	Potential (V vs. Li/Li$^+$)	$\overline{E_p}$ (eV)	x (EELS)
Nanometric Si	3.7	0.13	14.11 (0.09)	1.85
	3.6	0.18	15.51 (0.06)	1.38
	3.4	0.26	14.74 (0.14)	1.15
	3.3	0.30	13.87 (0.09)	2.16
	3.0	0.31	14.42 (0.15)	1.48
	3.0	0.32	14.39 (0.31)	1.52
	2.5	0.42	14.75 (0.08)	1.14
	2.3	0.43	15.03 (0.11)	0.88
	2.2	*0.37*	*14.98 (0.08)*	*0.92*
	1.9	0.49	15.57 (0.09)	0.53
	1.9	0.54	16.06 (0.08)	0.20
Micrometric Si	2.8	0.40	14.48 (0.16)	1.42
	2.2	0.42	14.85 (0.11)	1.04
	1.1	0.56	16.07 (0.12)	0.20

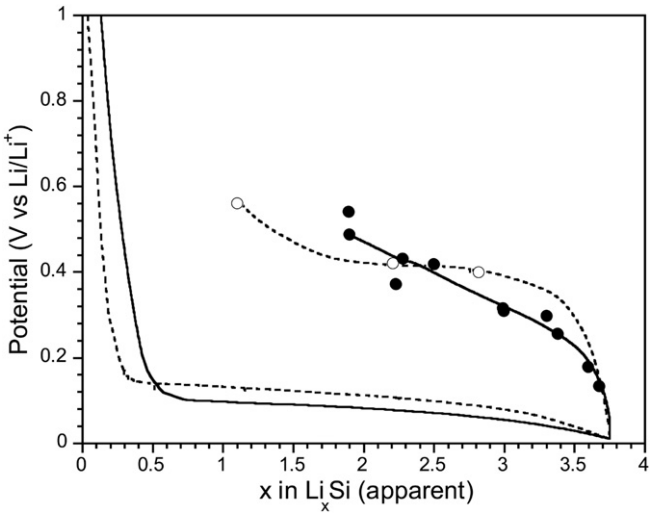

Fig. 2. Typical electrochemical curves for micro- and nano-Si electrodes as dash and full lines, respectively. Dots correspond to the samples analysed by EELS for micro-Si electrodes (empty circles) and nano-Si electrodes (filled circles).

throughout the entire composite electrode as seen in other conditions or systems [23,24], but rather at the nanoscale.

This result is clearly illustrated by Fig. 4a, which is characteristic of the morphology of the $x = 3.3$ composite electrode, where two areas probed by EELS are circled. The corresponding EELS spectra are given in Fig. 4b. The low-loss spectrum of the area labelled 2 is associated with a lithiated phase, whereas the spectrum of the area labelled 1 displays a peak characteristic of pure silicon around 17 eV. According to the diffraction pattern in the inset, this silicon particle is definitely crystalline. This observation occurred in many instances in this sample. Since dealloying of Si produces amorphous silicon [7], the presence of crystalline Si particles at the middle of the charge indicates that these particles were not lithiated at all during the first discharge. This conclusion is also supported by the fact that the crystalline nanoparticle observed in the TEM image (Fig. 4a, top) retains its pristine spherical shape. On the contrary, however, only 200 nm away from this particle, the part of the electrode corresponding to area 2 appears more chaotic, and is

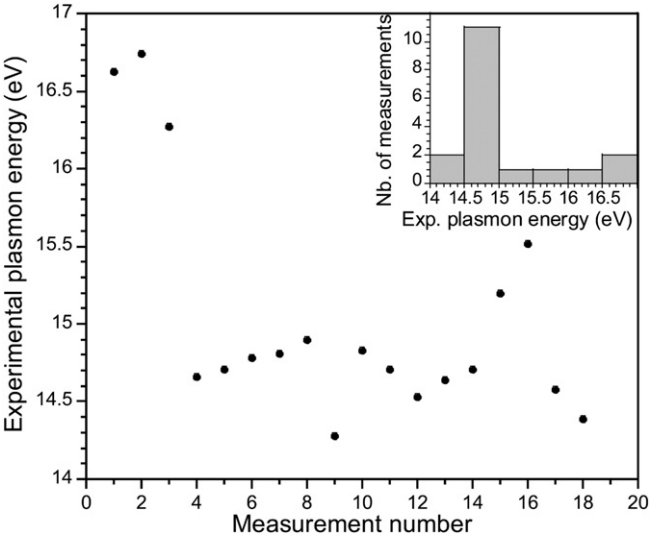

Fig. 3. Complete set of measured values for the plasmon energy of the $x = 2.5$ sample. A repartition by class is shown in the inset.

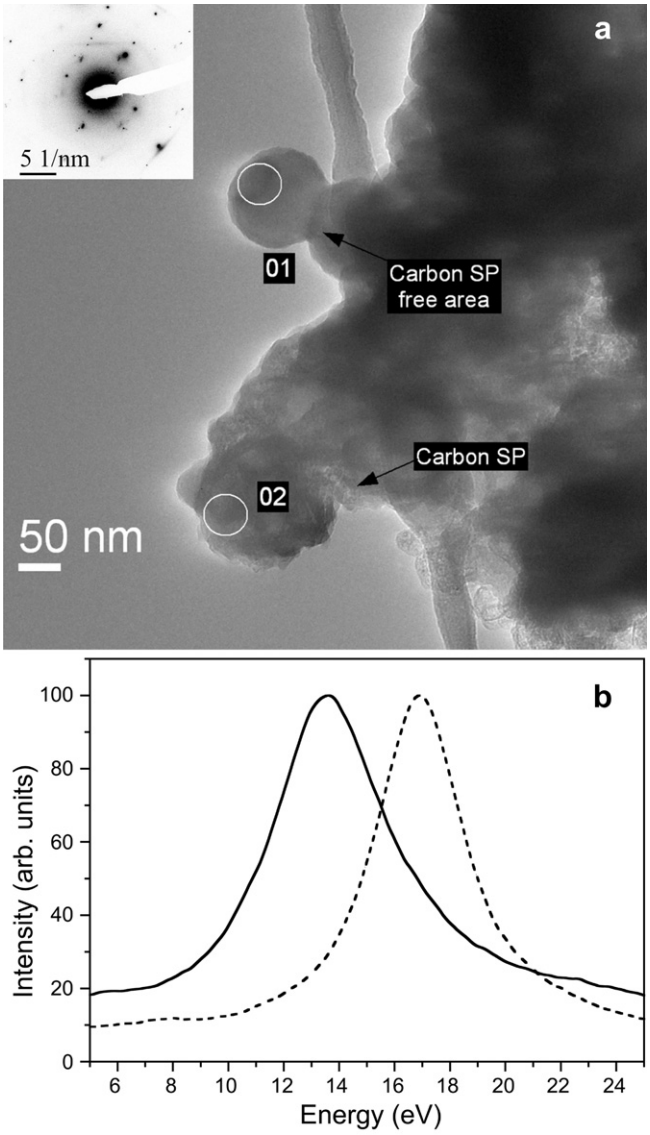

Fig. 4. (a) TEM image obtained on the nanometric Si-based electrode $x = 3.3$ along with the nano-diffraction pattern corresponding to area labelled 1 (inset). (b) Low-loss spectra of the areas labelled 1 (dashed line) and 2 (full line) in the TEM image (a).

amorphous and lithiated. Whereas the surface of the crystalline particle is very clean without detectable carbon SP (the conducting agent), this carbon is evidenced close to area labelled 2 (Fig. 4a). Since the incoming ions do not seem to be obstructed in accessing the particle, the electronic connection to the electrode network must be responsible for the absence of reaction. These results confirm that part of the material is inactive right from the first discharge of Si electrodes, and stress the crucial importance of an uniform and continuous electronic network, even below the 100 nm scale. A hierarchical architecture of the electrode is thus optimal in order to ensure both long- and short-range electronic connections, as previously demonstrated by Lestriez et al. [25].

3.2. Chemical composition of phases during delithiation

Due to the sizeable dispersion of the plasmon energy values observed within each sample (Fig. 3), some statistical processing was required to optimize exploitation of the data. First, data corresponding to pure Si were set aside when they deviated noticeably from other values, as observed in Fig. 3. They are due to unreacted particles and thus irrelevant to the alloy compositions. The Grubb's test [26], a statistical test for identifying outliers in a series, was then applied. This test quantifies how far out the doubtful outlier is situated with respect to other values, by calculating a sample criterion based on the mean and the standard deviation of the set of data. Comparison with a tabulated critical value, determined using the theory of random sampling, validated or rejected the tested value. For all samples, no more than one or two values were excluded, not counting the pure Si data. Subsequently, for every state of charge, means ($\overline{E_p}$) of the remaining plasmon energy values were calculated, as well as the corresponding mean standard deviation. Results are listed in Table 1.

Local compositions (x in Li_xSi) during the first charge were obtained by relating the determined plasmon energies to x, and this by way of the EELS database previously completed on Li_xSi alloys [14]. To this end, the reference data were fitted in the 12–17 eV range using the following second order polynomial function:

$$x(E_p) = 59.74 - 6.967E_p + 0.203E_p^2 \quad (1)$$

Local compositions can then be deduced for every state of charge. They are displayed in Fig. 5 as a function of the potential at which cells were stopped and dismantled, for both nano- and micro-Si electrodes. Values for micrometric Si-based electrodes are comparable to those found for nano-Si electrodes.

Right from the beginning of the charge, although only a small amount of lithium was removed from the $Li_{15}Si_4$ phase, a Li_xSi phase corresponding to $x \approx 2$ is immediately formed, as illustrated by the x(electrochem)=3.7 and 3.3 electrodes. Local compositions situated between 3.7 and 2 were never measured. This suggests the transformation of the $Li_{15}Si_4$ phase directly into a Li_xSi phase with $x \approx 2$, which is in good agreement with Dahn's group conclusions using XRD [6] and Mossbauer measurements [27]. The error on the $x = 2$ value can be estimated to be ± 0.3, combining both the uncertainty in Eq. (1) and the dispersion resulting from non-homogeneity (Fig. 5). Due to the preferential observation of thin areas using EELS, solely the Li_2Si phase is measured. Access to the core of the lithiated particles or the inner particles of clusters is limited and the $Li_{15}Si_4$ composition is not detectable.

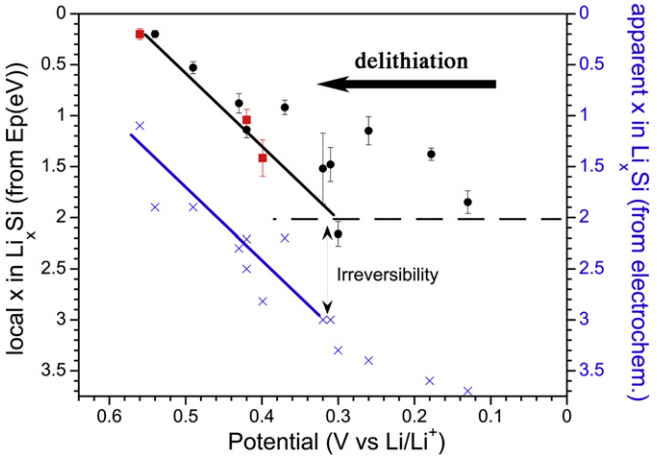

Fig. 5. Evolution, during the first delithiation, of the state of charge x in Li_xSi deduced from the plasmon peaks as a function of the potential at which the batteries were stopped for nanometric Si-based electrodes (black dots) and micrometric Si-based electrodes (red squares). States of charge deduced from electrochemical curves are also presented as a function of the potential for the same electrodes (crosses). Straight and dashed lines are drawn as guides to the eye. (For interpretation of the references to colour in this figure legend, the reader is referred to the web version of this article.)

After this two-phase domain, the local composition is found to vary almost linearly, corresponding well with a single phase process, which is expected to follow [6,28]. The transition from the two-phase domain to the solid solution one occurs for a potential around 0.30 V. This value is markedly different from that given by Li and Dahn, where the two-phase region exists almost until the end of the charge, with a potential around 0.45 V. One would usually consider this discrepancy to be indicative of a different dealloying process, due to the fact that Li and Dahn used micro-Si, whereas we have mainly used nano-Si. This, however, is not the case and is explained below.

In the case of micrometric Si (Fig. 2), the delithiation of Si leads to a distinct plateau on the voltage curve. For nano-Si, the delithiation curve exhibits no marked plateau but rather a sloppy voltage profile. Despite this fact, EELS experiments show that nano-Si based electrode cycling also occurs as a two-phase reaction. Even for nano-Si, a phase with an average $x = 2$ value coexists with the phase formed at full lithiation. Assuming as indicated by other researchers that this two-phase period is detrimental to the performance of the electrode [7], a large dispersion of local composition at the beginning of the charge is expected, and observed, even for the nano-Si electrode (Fig. 5, potential <0.4 V). Error bars on local EELS compositions are markedly smaller for potentials above 0.4 V indicating that the single phase process allows for the electrodes to recover a certain homogeneity towards the end of the delithiation.

Incremental capacity curves illustrate further similarities and differences between nano- and micro-Si based electrodes (Fig. 6). Both incremental capacities present a peak at ≈ 0.45 V in oxidation. In agreement with literature, this peak can be attributed to the crystalline $Li_{15}Si_4$ phase transforming into the amorphous Li_2Si phase [6]. In the case of nano-Si, at a lower potential (around 0.3 V), an intense and broad peak is observed. This tendency when particle size decreases is similar to the one evidenced in a-Si films as they get thinner [29–31]. Since we demonstrated that the phase being formed is Li_2Si at that potential (Fig. 5), this broad peak should also be attributed to the same compositional equilibrium $Li_{15}Si_4/Li_2Si$. The existence of an amorphous $Li_{15}Si_4$ phase is a fair assumption considering the final composition usually obtained, even for nano-Si, and the fact that heat treatment of the material at the end of lithiation promotes the crystallisation of $Li_{15}Si_4$ [32]. Most probably due to the poorly crystallized state, a highly defective $Li_{15}Si_4$ ("amorphous $Li_{15}Si_4$") has to be considered and the phase change occurs at lower potential. These conclusions should be linked to the incremental curves for $Li_{21}Si_5$ and $Li_{15}Si_4$ phases [33]. The observation of a small peak in the incremental capacity curve of nano-Si at 0.45 V could be due to the particle size dispersion of the sample possibly having larger crystals, or to a crystallisation assisted by the surrounding matrix or interfaces [34]. Our results are also in line with the competing interface and volume energies, which should favour low packing densities (i. e. amorphous phase) until a critical nucleus size is reached, as modelled by Zhang [34].

Finally, above approximately 0.35 V and up to 1 V, most of the very broad intensity measured both for nano- and micro-Si (Fig. 6) corresponds to the transformation of the Li_2Si phase to pure amorphous Si via a solid solution (Fig. 5).

In view of these results on local compositions, various conclusions can be drawn concerning the electrochemical process in silicon-based electrodes and the irreversibility observed along the first cycle. Firstly, our measurements for potentials around 0.55 V (Fig. 5) are characteristic of alloys with a very low lithium content. At the end of charge, the amount of lithium trapped in the alloy should thus be very limited. This local quantification confirms other measurements using ^{7}Li NMR [18] proposing that, in these electrodes and cycling conditions, disconnection of lithiated particles is not the main reason for irreversibility. Secondly, as shown in Fig. 5, x values deduced from electrochemistry in no way represent the chemical process occurring at the local scale, complicating interpretation of irreversibility based solely on these values. Thirdly, the shift between x values from electrochemistry and those from EELS is almost constant along the delithiation process and corresponds roughly to the first cycle irreversibility. This result seems to show that irreversibility is generated during the lithiation, and not during the delithiation. In these electrodes, the main issue is thus the SEI formation during lithiation. The SEI optimization, by the use of additives like FEC [35,36], is expected to greatly improve performance of these silicon-based electrodes.

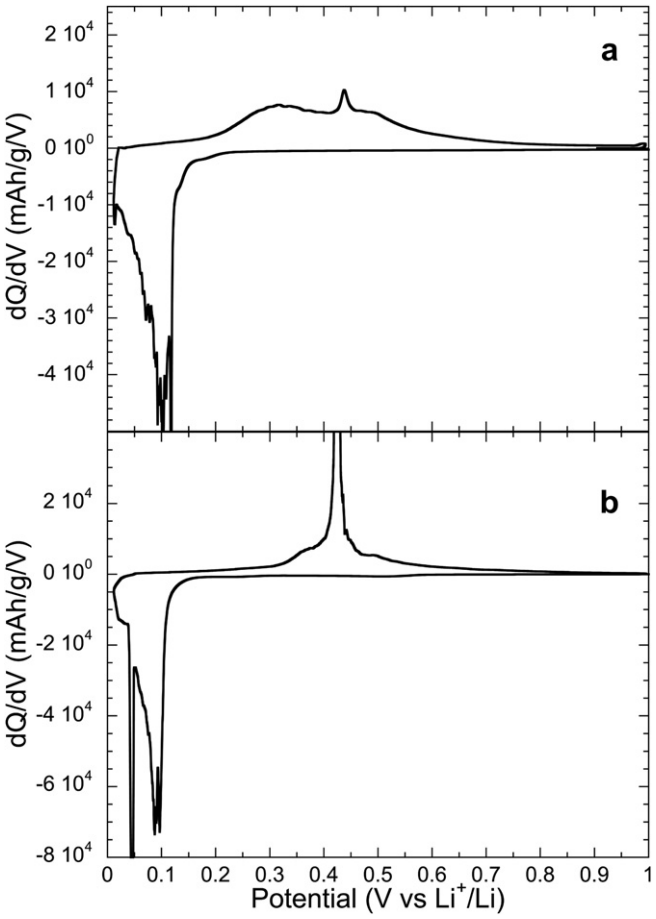

Fig. 6. Differential capacity dQ/dV vs potential for (a) a nano-Si electrode and (b) a micro-Si electrode.

4. Conclusions

Nanoscale experiments were performed using EELS to examine the variations of compositions occurring during the delithiation of Si practical electrodes. The effectiveness of the technique based on the measurement of alloy plasmons was further illustrated in this paper. Independently of the crystallisation state of the compound, local compositions could be obtained. Similar studies could be performed on conversion reaction systems where amorphous phases are often found. Inhomogeneities in composition existing at few hundred nanometre scale rather than in the whole electrode thickness were demonstrated. The optimization of the electrode formulation is thus a criterion crucial to the efficiency of the silicon electrodes. Despite this optimization, a sizeable dispersion of compositions at the beginning of the delithiation is observed for

various electrodes. Considering that such dispersion is very limited during the single phase process at the end of the charge, the evidenced biphasic process at the beginning of delithiation must play a role in these inhomogeneities.

For both nano-Si and micro-Si, our results validate previous studies performed during first delithiation by Li and Dahn on the coexistence of the $Li_{15}Si_4$ phase with a Li_xSi phase where x is estimated to be 2 ± 0.3, further followed by a solid solution extending from $x = 2$ to $x = 0$. Depending on the particle size, dissimilarities in the two-phase reaction have, however, been revealed. Micro-Si initial delithiation exhibits a well-defined two-phase process, while in the case of nano-Si, this process was smoothed due to the reduced scale of crystallisation. A coherent interpretation of EELS data and incremental capacity curves could thus be obtained.

Further lithiation/delithiation should bare very similar interpretation since it has been demonstrated that the two broad peaks present in the subsequent oxidations correspond directly to the two broad peaks observed in reduction [18,28]. However, the sizeable hysteresis between lithiation/delithiation average voltages could suggest different reaction pathways or additional interface-strain energy terms [34]. In order to provide a definitive answer, a similar study for the second lithiation would be very useful.

Although *in situ* experiments could supply more time dependent information on the lithiation/delithiation processes [37,38], in case they are modified by kinetics, this study demonstrates the usefulness of *ex situ* experiments in order to gain a specific point of view at practical electrode inhomogeneities.

Acknowledgements

Dr. J. Gaubicher is greatly acknowledged for fruitful discussion on the electrochemical process in these electrodes. Financial funding from the Agence Nationale de la Recherche (ANR) of France (BASILIC project) and the Natural Science and Engineering Research Council (NSERC) of Canada is acknowledged.

References

[1] H. Li, X. Huang, L. Chen, G. Zhou, Z. Zhang, D. Yu, Y. Jun Mo, N. Pei, Solid State Ionics 135 (2000) 181–191.
[2] P. Limthongkul, Y.-I. Jang, N.J. Dudney, Y.-M. Chiang, J. Power Sources 119–121 (2003) 604–609.
[3] L.Y. Beaulieu, K.W. Eberman, R.L. Turner, L.J. Krause, J.R. Dahn, Electrochem. Solid-State Lett. 4 (2001) A137–A140.
[4] D. Mazouzi, B. Lestriez, L. Roué, D. Guyomard, Electrochem. Solid-State Lett. 12 (2009) A215–A218.
[5] J.S. Bridel, T. Azais, M. Morcrette, J.M. Tarascon, D. Larcher, Chem. Mater. 22 (2010) 1229–1241.
[6] J. Li, J.R. Dahn, J. Electrochem. Soc. 154 (2007) A156–A161.
[7] M.N. Obrovac, L. Christensen, Electrochem. Solid-State Lett. 7 (2004) A93–A96.
[8] Y.-M. Kang, S.-M. Lee, S.-J. Kim, G.-J. Jeong, M.-S. Sung, W.-U. Choi, S.-S. Kim, Electrochem. Commun. 9 (2007) 959–964.
[9] S.-B. Son, J.E. Trevey, H. Roh, S.-H. Kim, K.-B. Kim, J.S. Cho, J.-T. Moon, C.M. DeLuca, K.K. Maute, M.L. Dunn, H.N. Han, K.H. Oh, S.-H. Lee, Adv. Energy Mater. 1 (2011) 1199–1204.
[10] X.H. Liu, H. Zheng, L. Zhong, S. Huang, K. Karki, L.Q. Zhang, Y. Liu, A. Kushima, W.T. Liang, J.W. Wang, J.-H. Cho, E. Epstein, S.A. Dayeh, S.T. Picraux, T. Zhu, J. Li, J.P. Sullivan, J. Cumings, C. Wang, S.X. Mao, Z.Z. Ye, S. Zhang, J.Y. Huang, Nano Lett. 11 (2011) 3312–3318.
[11] Y. Oshima, H. Sawada, F. Hosokawa, E. Okunishi, T. Kaneyama, Y. Kondo, S. Niitaka, H. Takagi, Y. Tanishiro, K. Takayanagi, J. Electron Microsc. 59 (2010) 457–461.
[12] V. Mauchamp, P. Moreau, L. Monconduit, M.-L. Doublet, F. Boucher, G. Ouvrard, J. Phys. Chem. C 111 (2007) 3996–4002.
[13] F. Cosandey, D. Su, M. Sina, N. Pereira, G.G. Amatucci, Micron 43 (2012) 22–29.
[14] J. Danet, T. Brousse, K. Rasim, D. Guyomard, P. Moreau, Phys. Chem. Chem. Phys. 12 (2010) 220–226.
[15] B. Key, R. Bhattacharyya, M. Morcrette, V. Seznéc, J.-M. Tarascon, C.P. Grey, J. Am. Chem. Soc. 131 (2009) 9239.
[16] P. Fallon, C.A. Walsh, University of Cambridge, England, 1996.
[17] R.F. Egerton, Electron Energy-Loss Spectroscopy in the Electron Microscope, Plenum Press, New York, 1996.
[18] Y. Oumellal, N. Delpuech, D. Mazouzi, N. Dupré, J. Gaubicher, P. Moreau, P. Soudan, B. Lestriez, D. Guyomard, J. Mater. Chem. 21 (2011) 6201–6208.
[19] J.H. Ryu, J.W. Kim, Y.-E. Sung, S.M. Oh, Electrochem. Solid-State Lett. 7 (2004) A306–A309.
[20] M. Smith, R.E. Garcia, Q.C. Horn, J. Electrochem. Soc. 156 (2009) A896–A904.
[21] C. Fongy, A.C. Gaillot, S. Jouanneau, D. Guyomard, B. Lestriez, J. Electrochem. Soc. 157 (2010) A885–A891.
[22] F. Tanguy, J. Gaubicher, D. Guyomard, Electrochem. Commun. 12 (2010) 561–564.
[23] F. Tanguy, J. Gaubicher, P. Soudan, N. Bourgeon-Martin, V. Mauchamp, D. Guyomard, Electrochem. Solid-State Lett. 10 (2007) A184–A188.
[24] L. Castro, R. Dedryvère, J.B. Ledeuil, J. Bréger, C. Tessier, D. Gonbeau, J. Electrochem. Soc. 159 (2012) A357–A363.
[25] B. Lestriez, S. Desaever, J. Danet, P. Moreau, D. Plee, D. Guyomard, Electrochem. Solid-State Lett. 12 (2009) A76–A80.
[26] F.E. Grubbs, Technometrics 11 (1969) 1–21.
[27] J. Li, A. Smith, R.J. Sanderson, T.D. Hatchard, R.A. Dunlap, J.R. Dahn, J. Electrochem. Soc. 156 (2009) A283–A288.
[28] M.N. Obrovac, L.J. Krause, J. Electrochem. Soc. 154 (2007) A103–A108.
[29] T.D. Hatchard, J.R. Dahn, J. Electrochem. Soc. 151 (2004) A838–A842.
[30] J. Graetz, C.C. Ahn, R. Yazami, B. Fultz, Electrochem. Solid-State Lett. 6 (2003) A194–A197.
[31] J.P. Maranchi, A.F. Hepp, P.N. Kumta, Electrochem. Solid-State Lett. 6 (2003) A198–A201.
[32] Y. Wang, J.R. Dahn, J. Electrochem. Soc. 153 (2006) A2188–A2191.
[33] J.Y. Kwon, J.H. Ryu, S.M. Oh, Electrochim. Acta 55 (2010) 8051–8055.
[34] W.-J. Zhang, J. Power Sources 196 (2011) 877–885.
[35] R.R. Garsuch, D.-B. Le, A. Garsuch, J. Li, S. Wang, A. Farooq, J.R. Dahn, J. Electrochem. Soc. 155 (2008) A721–A724.
[36] D. Mazouzi, N. Delpuech, Y. Oumellal, M. Gauthier, M. Cerbelaud, J. Gaubicher, N. Dupré, P. Moreau, D. Guyomard, L. Roué, B. Lestriez, J. Power Sources 220 (2012) 180–184.
[37] C.-M. Wang, X. Li, Z. Wang, W. Xu, J. Liu, F. Gao, L. Kovarik, J.-G. Zhang, J. Howe, D.J. Burton, Z. Liu, X. Xiao, S. Thevuthasan, D.R. Baer, Nano Lett. 12 (2012) 1624–1632.
[38] K. Karki, E. Epstein, J.-H. Cho, Z. Jia, T. Li, S.T. Picraux, C. Wang, J. Cumings, Nano Lett. 12 (2012) 1392–1397.